DIGITAL ACCESS TO
SCHOLARSHIP AT HARVARD

Long-Distance Spin-Spin Coupling via Floating Gates

(Article begins on next page)

Long-distance spin-spin coupling via floating gates

Luka Trifunovic,[1] Oliver Dial,[2] Mircea Trif,[1,3] James R. Wootton,[1] Rediet Abebe,[2] Amir Yacoby,[2] and Daniel Loss[1]

[1]*Department of Physics, University of Basel, Klingelbergstrasse 82, CH-4056 Basel, Switzerland*
[2]*Department of Physics, Harvard University, Cambridge MA, 02138, USA*
[3]*Department of Physics and Astronomy, University of California, Los Angeles, California 90095, USA*
(Dated: October 7, 2011)

The electron spin is a natural two level system that allows a qubit to be encoded. When localized in a gate defined quantum dot, the electron spin provides a promising platform for a future functional quantum computer. The essential ingredient of any quantum computer is entanglement—between electron spin qubits—commonly achieved via the exchange interaction. Nevertheless, there is an immense challenge as to how to scale the system up to include many qubits. Here we propose a novel architecture of a large scale quantum computer based on a realization of long-distance quantum gates between electron spins localized in quantum dots. The crucial ingredients of such a long-distance coupling are floating metallic gates that mediate electrostatic coupling over large distances. We show, both analytically and numerically, that distant electron spins in an array of quantum dots can be coupled selectively, with coupling strengths that are larger than the electron spin decay and with switching times on the order of nanoseconds.

I. INTRODUCTION

Spins of electrons confined to quantum dots provide one of the most promising platforms for the implementation of a quantum computer in solid state systems. The last decade has seen steady and remarkable experimental progress in the quantum control and manipulation of single spins in such nanostructures on very fast time scales down[1] to 200 ps and with coherence times of 270 μs.[2]

A large-scale quantum computer must be capable of reaching a system size of thousands of qubits, in particular to accommodate the overhead for quantum error correction.[3] This poses serious architectural challenges for the exchange-based quantum dot scheme,[4] since—with present day technology—there is hardly enough space to place the large amount of metallic gates and wires needed to define and to address the spin qubits. A promising strategy to meet this challenge is to implement long-range interactions between the qubits which allows the quantum dots to be moved apart and to create space for the wirings. Based on such a design we propose a quantum computer architecture that consists of a two-dimensional lattice of spin-qubits, with nearest neighbor (and beyond) qubit-qubit interaction. Such an architecture provides the platform to implement the surface code–the most powerful fault-tolerant quantum error correction scheme known with an exceptionally large error threshold of 1.1%.[5,6]

To achieve such long-range interactions we propose a mechanism for entangling spin qubits in quantum dots (QDs) based on floating gates and spin-orbit interaction. The actual system we analyze is composed of two double-QDs which are not tunnel coupled. The number of electrons in each double-QD can be controlled efficiently by tuning the potential on the nearby gates. Moreover, the electrons can be moved from the left to the right dot within each double-QD by applying strong bias voltage. Thus, full control over the double-QD is possible by only electrical means. The double-QDs are separated by a large distance compared to the their own size so that they can interact only capacitively. This interaction can be enhanced by using a 'classical' electromagnetic cavity, i.e., a metallic floating gate suspended over the two double-QDs, or a shared 2DEG lead between the qubits. The strength of the coupling mediated by this gate depends on its geometry, as well as on the position and orientation of the double-QDs underneath the gate. Finally, we show that spin-qubits based on spins-1/2[4] and on singlet-triplet states[7] can be coupled, and thus hybrid systems can be formed that combine the advantages of both spin-qubit types.

II. ELECTROSTATICS OF THE FLOATING GATE

The Coulomb interaction and spin-orbit interaction (SOI) enable coupling between spin-qubits of different QD systems in the complete absence of tunneling.[8–11] However, the Coulomb interaction is screened at large distances by electrons of the 2DEG and of the metal gates. Thus, the long-distance coupling between two spin-qubits is not feasible via direct Coulomb interaction. However, by exploiting long-range electrostatic forces, it was demonstrated experimentally[12,13] that QDs can be coupled and controlled capacitively via floating metallic gates over long distances. The optimal geometric design of such floating gates should be such that the induced charge stays as close as possible to the nearest QDs, and does not spread out uniformly over the entire gate surface. In other words, the dominant contributions to the total gate-capacitance should come from the gate-regions that are near the QDs. To achieve a strong qubit-qubit coupling there is one more requirement: the electric field induced on one QD needs to be sensitive to the changes of the charge distribution of the other QD. Thus, the charge gradient, $(\partial q_{ind}/\partial \boldsymbol{r})_{\boldsymbol{r}=0}$, needs to be large, where $\boldsymbol{r}$ is the position-vector of the point charge with the re-
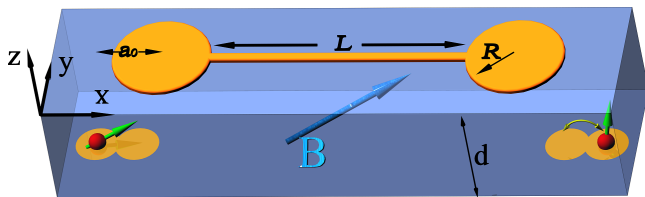
FIG. 1. Model system consisting of two identical double-QDs in the xy-plane and the floating gate between them. The gate consists of two metallic discs of radius R connected by a thin wire of length L. Each double-QD can accommodate one or two electrons, defining the corresponding qubit. Absence of tunneling between the separate double-QD is assumed; the purely electrostatic interaction between the electrons in the double-QDs leads to an effective qubit-qubit coupling. For the spin-1/2 qubit the coupling depends sensitively on the orientation of the magnetic field B. Here a_0 is the in-plane distance between a QD and the corresponding disc center, while d is vertical distance between the QD and the gate.

spect to the center of the respective QD. To fulfill these requirements we assume the floating gates consist of two metallic discs of radius R joined by a thin wire of length L.

Let us now investigate the optimal design by modeling the electrostatics of the floating gates. The electron charge in the QD induces an image charge of opposite sign on the nearby disc (ellipsoid), see Fig. 1. By virtue of the gate voltage being floating with respect to the ground, the excess charge is predominantly distributed on the distant metallic ellipsoid, thus producing an electric field acting on the second QD. In order to carry out the quantitative analysis of the electrostatic coupling, we make us of the expression for an induced charge on the grounded ellipsoidal conductor in the field of a point charge.[14] Electrostatic considerations imply that the coupling (gradient) is enhanced by implementing a flat-disc design of the gate. Thus, in what follows, we set the disc height to zero; to reach this regime in practice one only has to ensure that the disc height be much smaller than its radius. The expression for the induced charge (in the units of the electron charge) is then given by[14]

$$q_{ind}(\boldsymbol{r}) = \frac{2}{\pi}\arcsin(R/\xi_{\boldsymbol{r}}), \qquad (1)$$

where R is the radius of the disc, and a_0 is the distance between the QD and the ellipsoid centers (see Fig. 1). The ellipsoidal coordinate $\xi_{\boldsymbol{r}}$ is given by

$$2\xi_{\boldsymbol{r}}^2 = R^2 + d^2 + |\boldsymbol{a}_0 + \boldsymbol{r}|^2 \qquad (2)$$
$$+\sqrt{(R^2 + d^2 + |\boldsymbol{a}_0 + \boldsymbol{r}|^2)^2 - 4R^2|\boldsymbol{a}_0 + \boldsymbol{r}|^2}.$$

We emphasize that the induced charge depends only on the coordinate $\xi_{\boldsymbol{r}}$ of the external charge, as is readily seen from Eq. (1). This is one of the crucial points for the experimental realization of the qubit-qubit coupling. Thus, positioning the QD below the gate as in previous

setups[12] is not useful for the qubit-qubit proposed considered here, since $\partial q_{ind}/\partial\boldsymbol{r} \approx 0$. This fact, however, can be exploited to turn *on* and *off* the effective coupling between the qubits. Alternatively, one can use a switch that interrupts the charge displacement current through the floating gate and thus disables the build-up of charge gradients at the other disc.

Figure 2 depicts both the induced charged q_{ind}, as well as the charge variation $\partial q_{ind}/\partial r$ as a function of the horizontal distance a_0 between the center of the QD and the center of the gate. We see that for very small vertical distances $d \ll R$ the variation of the induced charge peaks at $a_0 \approx R$, reaching values as high as unity for $d = 0.1R$, and falls down quickly for a_0 larger or smaller than R. As mentioned above, this could be used as an efficient switching mechanism. However, as d increases to higher values, comparable to the disc radius R, the charge variation $\partial q_{ind}/\partial r$ flattens out over a wide range of in-plane distances a_0. This means that for larger depths $d \gtrsim \lambda$ of the quantum dot the switching mechanism turns out to be rather inefficient, even though the magnitude of the coupling is only weakly reduced ($\partial q_{ind}/\partial r \approx 0.3$ for $r \approx R$ and $d = 0.5R$). Nevertheless, the gates confining the QDs, as well as the 2DEG itself could lead to screening of the interaction between the QD and the floating gate, allowing for an improved switching even in this case.

Finally, by utilizing the expression for the electrostatic potential of a charged thin disc[14] we arrive at the expression for the electrostatic coupling

$$V(\boldsymbol{r}_1, \boldsymbol{r}_2) = \frac{\pi\alpha_q}{\kappa}\frac{e^2 q_{ind}(\boldsymbol{r}_1)q_{ind}(\boldsymbol{r}_2)}{R}, \qquad (3)$$

where κ is the dielectric constant, $\alpha_q = \frac{C_d}{C_w + 2C_d}$ is the charge distribution factor of the gate, and C_d and C_w are the capacitances of the discs and wire, respectively (see Appendix A). We mention that Eq. (3) is derived in the limit when the floating gate is immersed in the dielectric, and it provides a lower bound for $V(\boldsymbol{r}_1, \boldsymbol{r}_2)$ in the realistic case when the floating gate sits on top of the dielectric.

III. QUBIT-QUBIT COUPLING

Next, we consider the coupling between qubits. These can be for either single- or double-QDs. The two-qubit system with the floating gate is well described by the Hamiltonian

$$H = V + \sum_{i=1,2} H_{qubit}^i, \qquad (4)$$

where V describes the electrostatic coupling between the distant charges in the qubits and is given by Eq. (3), and H_{qubit}^i stands for either the single-QD or double-QD Hamiltonian[9,15]

$$H_{QD} = H_0 + H_Z + H_{SO}, \qquad (5)$$
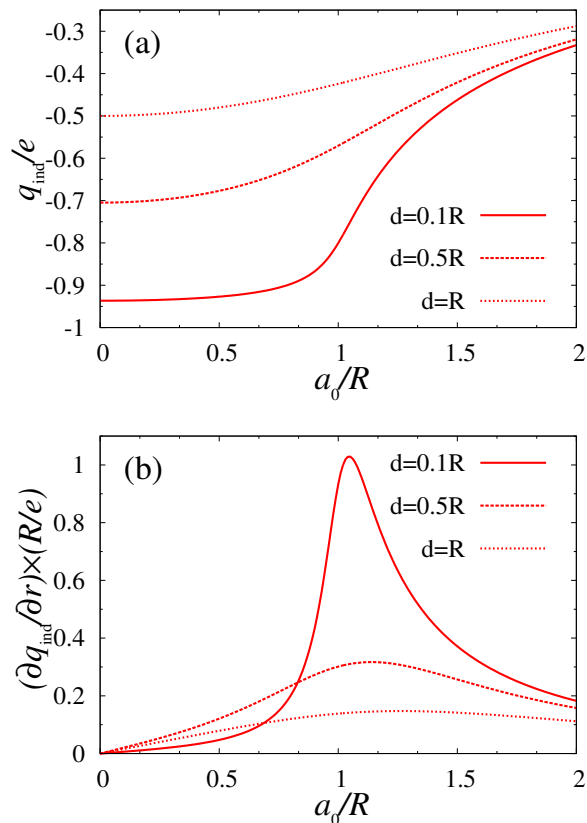$$H_{DQD} = J\,\boldsymbol{S}_1 \cdot \boldsymbol{S}_2 + H_Z^1 + H_Z^2. \qquad (6)$$

FIG. 2. (a) The dependence of the induced charge, q_{ind}, and (b) of the derivative of the induced charge, $\partial q_{ind}/\partial r$, on a_0 at $r = 0$, i.e. the in-plane distance from the center of the cylindrical gate to the center of the QD. We plot these two quantities for several vertical distances d between the QD and the gate: $d/R = 0.1$, 0.5, 1, corresponding to the full, dashed and dotted lines, resp..

Here, $H_0 = p_i^2/2m^* + m^*(\omega_x^2 x_i^2 + \omega_y^2 y_i^2)/2$ is the energy of an electron in dot i described by a harmonic confinement potential, m^* being the effective mass and $\hbar\omega_{x,y}$ the corresponding single-particle level spacings. For a single-QD $H_Z = g\mu_B \boldsymbol{B} \cdot \boldsymbol{\sigma}/2$, stands for the Zeeman coupling, with $\boldsymbol{\sigma}$ the Pauli matrix for the spin-1/2, and both Rashba and Dresselhauss spin-orbit interactions

$$H_{SO} = \alpha(p_x\sigma_y - p_y\sigma_x) + \beta(-p_x\sigma_x + p_y\sigma_y), \quad (7)$$

where α (β) is the Rashba (Dresselhauss) spin-orbit interaction strength. The double-QD is described by an effective Heisenberg model,[15] Eq. (6), with $\boldsymbol{S}_i$ being the spin in the double-QD. In what follows we assume the floating gate to be aligned along the x-axis, see Fig. 1.

A. Singly occupied double-QDs

We start by considering two single-QD qubits. Let us first give a physical description of the qubit-qubit coupling. The purely electrostatic coupling between the QDs

involves only the charge degrees of freedom of the electrons. Within each QD the spin degree of freedom is then coupled to the one of the charge via spin-orbit interaction. Hence, we expect the effective spin-spin coupling to be second order in the SOI and first order in the electrostatic interaction. In fact, one has also to assume Zeeman splitting to be present on at least one QD in order to remove the van Vleck cancellation.[16,17]

Proceeding to a quantitative description, we assume the spin-orbit strength to be small compared to the QD confinement energies $\hbar\omega_{x,y}$. Following Refs. 9 and 17, we apply a unitary Schrieffer-Wolff transformation to remove the first order SOI terms. The resulting Hamiltonian has decoupled spin and orbital degrees of freedom (to second order in SOI), with the effective qubit-qubit coupling (see Appendix A), with

$$H_{S-S} = J_{12}(\boldsymbol{\sigma}_1 \cdot \boldsymbol{\gamma})(\boldsymbol{\sigma}_2 \cdot \boldsymbol{\gamma}) \quad (8)$$

$$J_{12} = \frac{m^*\omega_{x,12}^2 E_Z^2}{2(\omega_x^2 - E_Z^2)^2}, \quad (9)$$

where $\boldsymbol{\gamma} = (\beta\cos 2\gamma, -\alpha - \beta\sin 2\gamma, 0)$; γ being the angle between the crystallographic axes of the 2DEG and the xyz-coordinate system defined in Fig. 1. Here we assumed for simplicity that the magnetic field is perpendicular to the 2DEG substrate, with $E_Z = g\mu_B B$ the corresponding Zeeman energy (assumed also the same for both dots). However, neither the orientation nor the possible difference in the Zeeman splittings in the two dots affect the functionality of our scheme (see Appendix A for the most general coupling case). We mention that the spin-spin interaction in Eq. (8) is of Ising type, which, together with single qubit gates forms a set of universal gates (see below).

All information about the floating gate coupling is embodied in the quantity

$$\omega_{x,12}^2 = \pi\alpha_q\alpha_C\left(\frac{\partial q_{ind}}{\partial\tilde{x}}\right)_{\boldsymbol{r}=0}^2\omega_x^2, \quad (10)$$

where $\alpha_C = e^2/(\kappa R\hbar\omega_x)$, and $\tilde{x} = x/\lambda$ (λ is the QD size). It is interesting to note that the derived coupling, Eq. (10), is independent of the orbital states of the QDs, and thus, insensitive to charge fluctuations in the dots. More importantly, the coupling has only a weak dependence on the wire length L—through the capacitance ratio α_q.

Next, we give estimates for the qubit-qubit coupling for GaAs and InAs QDs. Taking the spin-orbit strength for GaAs semiconductors $\lambda/\lambda_{SO} \simeq 10^{-1}$, and assuming $E_{Z1} \simeq E_{Z2} \equiv E_Z \simeq 0.5\hbar\omega_x$ ($B = 2T$ and $\hbar\omega_x \simeq 1meV$), we obtain $H_{s-s} \simeq \alpha_q\alpha_C(\partial q_{ind}/\partial\tilde{x})_{\boldsymbol{r}=0}^2 \times 10^{-7}eV$. The electrostatic coupling strongly depends (like d^{-2}) on the vertical distance between the gate and the QDs. Typically, $d \simeq \lambda$, and one obtains using Eq. (1) maximal coupling $H_{s-s} \simeq 10^{-11}-10^{-10}eV$ (for $R = 1.6\lambda$, $L = 10\mu m$, and $R_w = 30nm$ leading to $\alpha_q = 0.02$; $a_0 = 1.9\lambda$). Although, it is experimentally challenging to decrease d to

a value of about $10nm$, the gain would be a significantly stronger coupling $10^{-9} - 10^{-8}eV$ (for $R = 0.17\lambda$ and $a_0 = 0.2\lambda$). Moreover, if a semiconductor with larger spin-orbit coupling is used—such as InAs ($\lambda/\lambda_{SO} \simeq 1$)—the coupling is increased by two orders of magnitude compared to GaAs, reaching the μeV-regime. Quite remarkably, these values almost reach within the exchange strengths range, $J_{exc} \sim 10 - 100\mu eV$, occurring in typical GaAs double quantum dots.[1,4] Actually, for realistic devices—as presented in the Sec. VI—the coupling is almost two orders of magnitude larger then the estimates presented herein. This discrepancy is not very surprising and it is mainly due to our pessimistic treatment of the dielectric, and the sensitivity of the electric field gradient to geometry of the surrounding gates.

B. Hybrid spin-qubits

A number of different spin-based qubits in quantum dots have been investigated over the years,[18] each with its own advantages and challenges. The most prominent ones are spin-1/2 and singlet-triplet spin qubits. Here, we show that these qubits can be cross-coupled to each other and thus hybrid spin-qubits can be formed which open up the possibility to take advantage of the 'best of both worlds'.

We model the hybrid system by a single- and a double-QD qubit, described by Eqs. (5) and (6), respectively. The single-QD and the floating gate act as an electric field, leading to the change in the splitting between the logical states of the double-QD spin-qubit, $J \to J + \tilde{x}_e \delta \tilde{J}$,[15] with $x_e = \tilde{x}_e \lambda$ being the x-coordinate of the electron in the single-QD and

$$\delta \tilde{J} = \frac{3}{\sinh(2\tilde{l})} \frac{\omega_{x,12}^2}{\tilde{l}\omega_D^2} \epsilon .\qquad (11)$$

Here, ω_D is the confinement energy in the DQD, $\tilde{l}$ is the distance between the double-QD minima measured in units of a QD size λ. The previous formula is valid for the regime $\epsilon \gtrsim \omega_D$.

In order to decouple spin and orbital degrees of freedom, we again employ a Schrieffer-Wolff transformation and obtain the hybrid coupling in lowest order (see Appendix B)

$$H_{hybrid} = \frac{3\mu g \, \delta \tilde{J}(\boldsymbol{\gamma} \times \boldsymbol{B}) \cdot \boldsymbol{\sigma}}{4(\omega_x^2 - E_{Z1}^2)\lambda} \tau_z .\qquad (12)$$

Here, τ_z is a Pauli matrix acting in the pseudo-spin space spanned by the logical states of the singlet-triplet qubit. It should be noted that the sign of this coupling can be manipulated by changing the sign of the detuning voltage ϵ. As an estimate, we can write $H_{hybrid} \simeq \left(\frac{\omega_{x,12}}{\omega_x}\right)^2 \frac{E_Z}{\omega_D} \frac{a_B}{\lambda_{SO}} \epsilon$. Assuming the parameters cited in the previous section for the GaAs-QDs we obtain the estimate $H_{S-s} \simeq 10^{-10} - 10^{-9}eV$. Reducing the distance d

or using InAs-QDs we can gain one order of magnitude more in the coupling.

C. Doubly occupied double-QDs

To complete our discussion about the qubit-qubit couplings, we now consider two double-QDs coupled via the floating gate. As already noted, owing to the different charge distributions of the logical states in the double-QD, the SOI term is not needed for the qubit-qubit coupling.[10] Certainly, the SOI exists in double-QDs but its effect on the ST splitting can be neglected. Below only a rough estimate of the coupling is provided, while the detailed analysis can be found in Ref. 10.

We assume both double-QDs to be strongly detuned, thereupon the singlet logic state is almost entirely localized on the lower potential well of the double-QD. The electrostatic energy difference between the singlet-singlet and triplet-triplet system configurations gives the rough estimate of the qubit-qubit coupling, $H_{S-S} \simeq V(R, R) - V(R + l, R + l)$. Taking the distance between the double-QD minima $l \simeq R$ and the same GaAs parameters as before, we finally obtain the estimate $H_{S-S} \simeq 10^{-5} - 10^{-6}eV$. As can be seen from Fig. 2, reducing d to $10nm$ increases the coupling five times.

IV. SCALABLE ARCHITECTURE

One central issue in quantum computing is scalability, meaning that the basic operations such as initialization, readout, single- and two-qubit gates should not depend on the total number of qubits. In particular, this enables the implementation of fault-tolerant quantum error correction,[3] such as surface codes where error thresholds are as large as 1.1%.[5,6]

To this end, the architecture of the qubit system becomes of central importance.[19] Making use of the electrostatic long-distance gates presented above, we now discuss two illustrative examples for such scalable architectures.

A. Design with floating metal gates

In the first design we propose here, the metallic gates above the 2DEG are utilized for qubit-qubit coupling, while the switching of the coupling is achieved by moving the QDs (see Fig. 3). Only the coupling between adjacent QDs is possible in this design. Without this constraint, the induced charge due to nearby QDs would be spread over the whole system, resulting in an insufficient qubit-qubit coupling.

The actual virtue of the setup is its experimental feasibility, as suggested by recent experiments.[12,13] However, as explained in Sec. II, a minor but crucial difference here is that the qubit-qubit coupling depends not on the
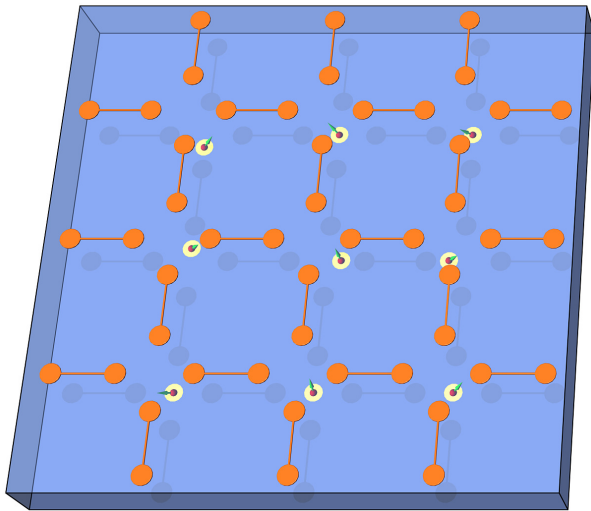
FIG. 3. Quantum computer architecture using metallic floating gates on top of a 2DEG. The electrostatic long-range coupling is confined to adjacent qubits. Turning on (off) the qubit-qubit interaction is achieved by moving a qubit close to (away from) the corresponding metal disc. This architecture allows for parallel switching.

charge itself but rather on its gradient, in contrast to earlier designs.[12,13] This requires the dots to be positioned off the disc-center.

In order to complete our quantum computer design, we have to equip our system with a fast switch. The discussion in Sec. II is relevant therefore, because the coupling can be turned *off* (*on*) by moving a QD away (towards) the corresponding floating gate, see Fig. 2. The spatial change of the quantum dot induces an electric response in the metallic floating gate on a time scale roughly given by the elastic mean free time (at low temperatures). This is the time it takes to reach the new electronic equilibrium configuration that minimizes the electrostatic energy. Since for a typical metal this time is on the order of tens of femtoseconds, this response time poses no limitations, being much faster than the effective switching times obtained in the previous sections.

B. All-in-2DEG design

We now consider a setup where are all elements of the qubit-network, including the floating connector gates, are implemented in the 2DEG itself. This will allow us to extend the above design in an essential way, namely to implement a switching mechanism inside the connectors themselves which is potentially fast and efficient (with a large on/off ratio). There are two attractive features coming with such a design. First, the qubit-qubit coupling is now controlled by the connector switch only, while the quantum dots with the spin-qubits can be left fixed, thereby reducing the source of gate errors. Second, this design allows for coupling beyond nearest neighbor

qubits, which is beneficial for the error threshold in fault-tolerant quantum error correction schemes.[19]

The proposed network is shown in Fig. 4 where the floating gates are formed within the 2DEG in form of discs connected by quantum wires. The discs themselves can be considered as large quantum dots containing many electrons ($\sim 50 - 100$) so that (quantum) fluctuations are negligibly small. Parts of the network are then connected or disconnected by locally depleting these wires with the help of a standard quantum point contact.[1] This suppresses the displacement of charges very quickly and efficiently. The electrostatics of such semiconductor gates is essentially the same as the previously discussed metallic one. Indeed, the number of electrons in the 2DEG-defined network can be fixed, thus the gate behaves as floating. Again, the minimal switching time is limited roughly by the elastic mean free time (at low temperatures), which for a typical GaAs 2DEG is on the order of tens of picoseconds.

The single spin control required for completing the universal set of gates in our proposal can be implemented in both setups through ESR,[20] or purely electrically via EDSR,[21–23] which is more convenient for our electrostatic scheme. The time scales achieved are on the order of 50 ns, much shorter than the spin relaxation and decoherence times.[21–23]

C. Design based on 1D nanowire quantum dots

The floating gate architecture efficiency is strongly dependent on the strength of the SOI experienced by the electrons in the QDs, which have to be large enough to overcome the spin decoherence rates. InAs nanowires are such such strong SOI materials, with strengths larger by an order of magnitude than in GaAs 2DEG.[24] Moreover, the electron spins in QDs created in these nanowires show long coherence times[23] and can be controlled (electrically) on times scales comparable to those found for the electron spin manipulation in GaAs gate defined QDs.[23]

In Fig. 5 we show a sketch of an architecture based on nanowires containing single or double QDs. Typical examples for such wires are InAs[23,24] or Ge/Si[25,26] nanowires, Carbon nanotubes,[27–30] etc. The default position of a QD is chosen so that the coupling to any of the surrounding gates is minimal. Neighboring QDs in the same nanowire are coupled by a vertical metal gate, while QDs in adjacent nanowires by a horizontal metal gate. The electron in a given QD can be selectively coupled to only two of the surrounding gates by moving it (via the gates that confine the electrons) in regions where the electric field gradient for the induced charge is maximum on these two 'active' gates, while negligible for the others two 'passive' gates. The other QD partner in the coupling is moved towards one of the 'active' gates thus resulting in a qubit-qubit coupling. Note that there are in total three 'active' gates, but only one of them is shared by both QDs, thus allowing selective coupling of
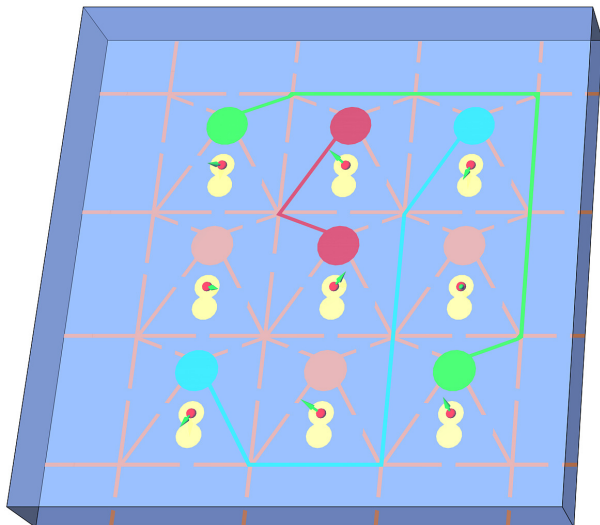
FIG. 4. All-in-2DEG design: the qubits and the floating connector gates are all implemented within the same 2DEG. The spin-qubits (green arrow) are confined to double quantum dots (small yellow double circles) and are at a fixed position with maximum coupling strength to the floating gate (big disc) (see Fig. 2). The network consists of quantum channels (lines) that enable the electrostatic coupling between discs (large circles) so that two individual qubits at or beyond nearest neighbor sites can be selectively coupled to each other. In the figure shown are four pairs of particular discs that are connected by quantum channels (full lines), while the remaining discs (red) are disconnected from the network (interrupted red lines) The discs can be considered as large quantum dots containing many electrons. The quantum wires can be efficiently disconnected (interrupted lines) by depleting the single-channel with a metallic top gate (not shown). This architecture allows for parallel switching.

any nearest neighbor pair in the network.

The spin coupling mechanism as well as the 2D geometry are similar to the previous 2DEG GaAs QDs designs, showing the great flexibility of the floating gate architecture. As before, the spin-qubits can be manipulated purely electrically, via the same gates that confine the QDs.[23] We mention also that the gate geometry (dogbone like) shown in Fig. 5 is not optimized to achieve the best switching ratio, more asymmetric gate geometries possibly leading to better results.

D. Spin qubit decoherence and relaxation

Decoherence and relaxation are ones of the main obstacles to overcome in building a quantum computer. The main source of qubit decay in typical GaAs quantum dots comes from nuclear spins and phonons (via spin orbit interaction), and has been studied in great detail theoretically and experimentally, see e.g. 31. The longest relaxation and decoherence times measured are about $T_1 \sim 1s$[32] and $T_2 \sim 270\mu s$,[2] respectively. Exactly the
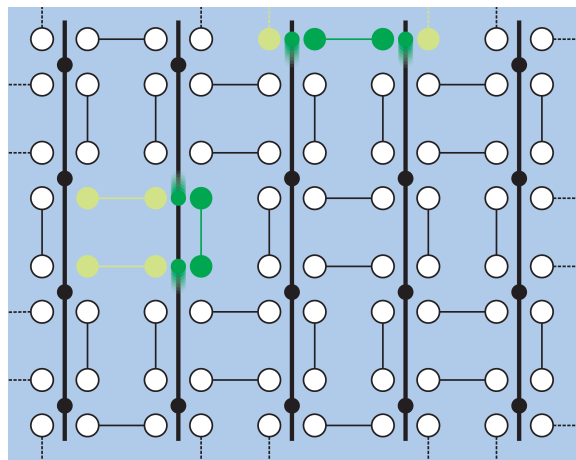

FIG. 5. Architecture based on nanowire QDs coupled by metallic gates. The spin qubits are confined to QDs (black dots) on nanowires. The nanowires form a parallel array (vertical black lines). The coupling between neighboring spin-qubits is enabled by floating metal gates (white) positioned either parallel to the wires thus coupling QDs created in the same wire, or perpendicular to the wires thus coupling QDs created in adjacent nanowires. By using external gates (not shown) to move the dots along the nanowires (shaded colors) it is then possible to selectively couple one particular QD to only two surrounding gates ('active' gates; green and yellow). The other QD partner couple to one of these 'active' gates also (green), thus resulting in a selective coupling of the desired nearest neighbor pair.

same qubit decay mechanisms also apply here, except one new source coming from the Nyquist noise of the floating metallic gates. However, this problem has been studied in great detail in Ref. 33 and no major impact on the decoherence time was found. Even if Nyquist noise were a problem, it could be further reduced by using superconducting gates in lieu of normal metal ones.

V. IMPLEMENTATION OF TWO-QUBIT GATES

Since the Hamiltonian of Eq. (8) is entangling, it can be used to implement two-qubit gates. Here we consider the CNOT gate, widely used in schemes for quantum computation.[5,6] The Hamiltonian for two single-QD qubits interacting via the floating gate is the sum of H_{S-S} and the Zeeman terms. The strength of the latter in comparison to the former allows us to approximate the Hamiltonian by $H' = J_{12}|\gamma|^2(\sigma_x^1\sigma_x^2 + \sigma_y^1\sigma_y^2)/2 + E_z(\sigma_z^1 + \sigma_z^2)/2$, for which qubit-qubit interaction and Zeeman terms commute. The CNOT gate, C, may then be

realized with the following sequences,

$$C = \sqrt{\sigma_z^1}\,\sqrt{\sigma_x^2}\,\mathcal{H}^1 e^{i(\sigma_z^1+\sigma_z^2)E_z t}e^{-iH't}$$
$$\sigma_x^1 e^{i(\sigma_z^1+\sigma_z^2)E_z t}e^{-iH't}\,\sigma_x^1\,\mathcal{H}^1, \tag{13}$$

$$C = \sqrt{\sigma_z^1}\,\sqrt{\sigma_x^2}\,\mathcal{H}^1\,\sigma_x^2\,e^{-iH't/2}\,\sigma_x^1\sigma_x^2\,e^{-iH't/2}$$
$$\sigma_x^2\,e^{-iH't/2}\,\sigma_x^1\sigma_x^2\,e^{-iH't/2}\,\mathcal{H}^1 \tag{14}$$

where $t = \pi/(4J_{12}|\boldsymbol{\gamma}|^2)$ and $\mathcal{H}$ denotes the single qubit Hadamard rotation. These sequences require two and four applications of the floating gate, respectively. More details on their construction can be found in Appendix C. Since H' is only an approximation of the total Hamiltonian, these sequences will yield approximate CNOTs. Their success can be characterized by the fidelity, as defined in Appendix C. For realistic parameters, with the Zeeman terms an order of magnitude stronger than the qubit-qubit coupling, the above sequences yield fidelities of 99.33% and 99.91% respectively. For two orders of magnitude between the Zeeman terms and qubit-qubit coupling the approximation improves, giving fidelities of 99.993% and 99.998%, respectively. These are all well above the fidelity of 99.17%, corresponding to the threshold for noisy CNOTs in the surface code.[6] Hence, despite the difference in error models, we can be confident that the gates of our scheme are equally useful for quantum computation.

VI. NUMERIC MODELING OF REALISTIC DEVICES

In the previous sections, a number of practical concerns related to the construction of working devices were neglected; most notably, the existence of the metallic gates used to define the quantum dots themselves and the presence of undepleted 2DEG outside of the quantum dots. These have finite capacitances to the coupler, shunting away some of the charge that would otherwise contribute to the inter-qubit interaction. To confirm that substantial couplings can still be attained at large distances with these limitations, we have performed numeric simulations of devices with realistic geometries similar to currently in-use ST spin qubits. A typical simulated geometry is included in Fig. 6. The gate and heterostructure design is identical to a functional device currently being characterized, and the boundaries of the 2DEG and placement of the electrons within the dot are estimates guided by experimentally measured parameters. Each quantum dot is modeled as a fixed charge metallic disc 50 nm in diameter within the 2DEG. While unsophisticated, this suffices to estimate the practicality of this scheme.

We define the coupling between two ST qubits as the change in detuning in one ST qubit induced by the transfer of a full electron from one dot to the other dot in a second ST qubit. For our reference ST qubit design with the two qubits physically adjacent to each other and no coupler (680 nm center-to-center), we calculate a coupling
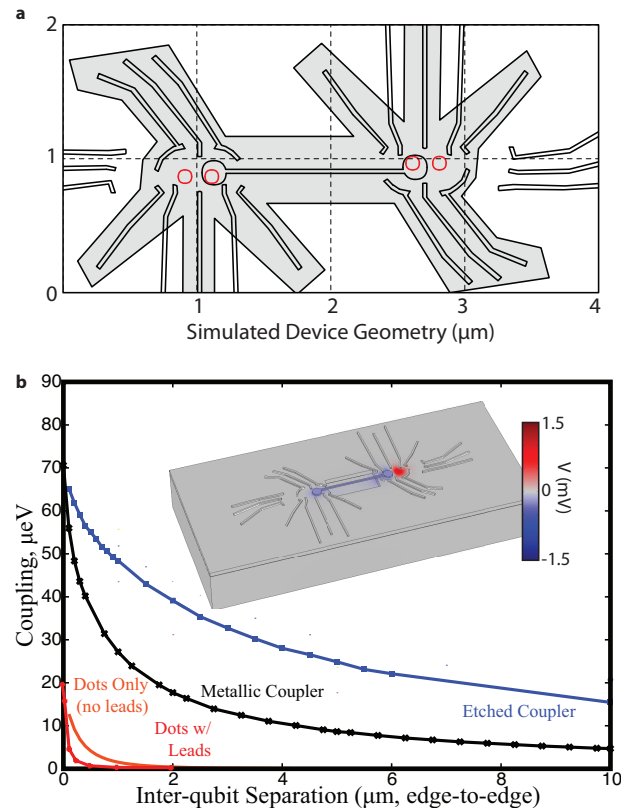

FIG. 6. Numeric simulation confirm the efficacy of the design for S-T qubits; addition of a metallic coupler (crosses) increases coupling more than 3-fold for closely spaced dots, and greatly extends the range of the coupling. (a) The simulated device with a separation of 1 μm and an etched coupler. 2DEG underneath the shaded region is treated as depleted, while red circles show the locations of the individual quantum dots within the simulation. (b) Coupling strength as a function of separation for the ST qubits in free space (smooth curve), qubits including leads and 2DEG but without a coupler (red +), including a metallic coupler (black crosses), and additionally etching a trench around the coupler to deplete the 2DEG underneath (blue squares). Inset: Electrostatic potential (color scale) at the sample surface shows the impact of the coupler on a device with a 1 μm separation.

of 20μeV. As the qubits are separated, the coupling vanishes rapidly as the 2DEG in between the qubits screens the electric field; it is reduced by an order of magnitude if the dots are separated by an additional 250 nm. This rapid falloff makes the gate density needed for large scale integration of these qubits problematic.

Addition of a floating metallic coupler of the type described herein increases the coupling at zero separation to 70μeV and allows the qubits to be separated by more than 6μm before the coupling drops to the level seen for two directly adjacent qubits. We can further improve upon this coupling by etching the device in the vicinity of the coupler, reducing the shunt capacitance of the coupler to the grounded 2DEG between the devices.

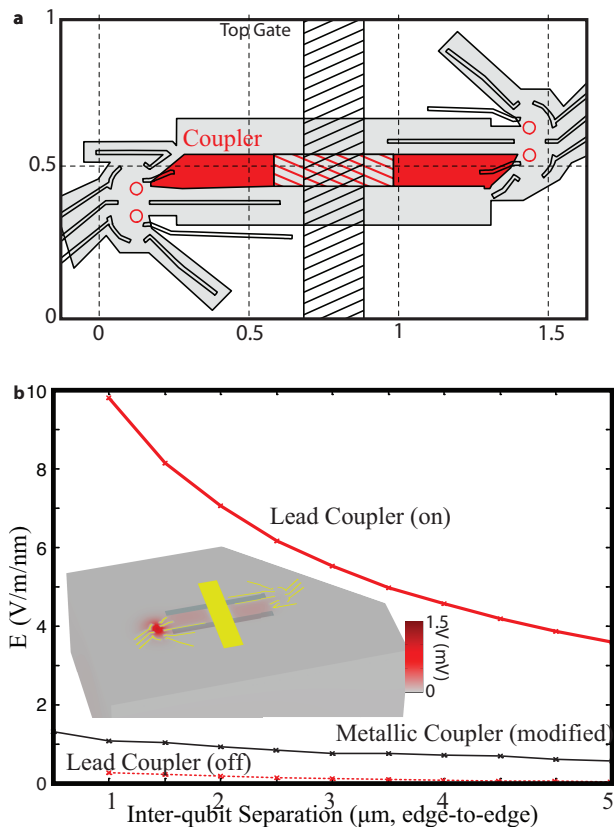For the case of single spins this metallic coupler is mod-

FIG. 7. Simulations of single-spin qubits show appreciable coupling strengths, even over distances of several microns. While the metallic coupler design of Fig. 6 modified to place the quantum dots at the edges of the couplers is effective (black crosses in b), an all-in-2DEG design where one of the leads of the qubit acts as a coupler (red region in a) provides dramatically enhanced coupling (solid red lines in b). The coupler is deactivated by a metallic top gate (black hatched region in a), modeled by removing the hatched section of the coupler. Doing so reduces inter-qubit coupling by over an order of magnitude (dashed red lines in b).

lectively turn this coupling on and off. The reduction in coupling in the off state is more than an order of magnitude, and can be further improved by increasing the size of the depleted region.

VII. CONCLUSIONS

We proposed and analyzed an experimentally feasible setup for implementing quantum gates in an array of spin qubits localized in gate-defined quantum dots based on the interplay of the Coulomb repulsion between the electrons, SOI and externally applied magnetic fields. As opposed to the current schemes based on direct exchange, here there is no need for electron tunneling between the quantum dots, thus bringing the scheme within experimental reach based only on current spin-qubit technology.

We showed, both analytically and numerically, that using either metallic floating gates in the shape of a dog-bone, or the 2DEG itself acting as a metallic gate, long-range spin-spin coupling is achieved, with coupling strengths exceeding the spin decay rates. Moreover, the coupling can be selectively switched *on* and *off* between any pairs of qubits by only local qubit manipulation, allowing entangling quantum gates such as the CNOT to be performed accurately and efficiently. The two-dimensional architecture based on the design provides a platform for implementing the powerful surface code.

The electrostatic scheme proposed here is a step forward towards an efficient implementation of gates also between hybrid qubits, like ST qubit, hole-spin qubits, or even superconducting qubits. This opens up new avenues for a future working hybrid quantum computer based not on one, but several types of qubits.

ified to place the quantum dots at the edges of the coupler rather than under the discs. We define the coupling in this case as the electric field in V/m induced on one qubit in response to 1nm of motion of the electron on the other qubit. We continue to find substantial couplings even at large separations (Fig. 7). However, in this case we find we can further improve couplings by moving to the all-in-2DEG design where one of the leads of the quantum dot is used as the coupler (Fig. 7 a). Using the lead in this fashion should be harmless; no current is driven into the lead during qubit manipulations. The lead (colored region) is modeled as a metallic strip at the level of the 2DEG. Due to the close proximity of the lead to the qubit as well as the sharp electric field gradients near the point of the lead, we find strongly enhanced coupling for this lead coupler over the floating metallic coupler for single spin qubits. By depleting part of the lead coupler using a metallic top gate (yellow region), it is possible to se-

Appendix A: SPIN-SPIN COUPLING - singly occupied double-dots

In this section we derive explicitly the effective spin-spin coupling. The spin-orbit interaction (SOI) Hamiltonian H_{SO} is assumed to be small compared to both the orbital Hamiltonian $H_0 + V$ and the Zeeman coupling H_Z, so that we can treat it in perturbation theory. The method of choice for the perturbation theory is based on the Schrieffer-Wolff (SW) transformation, following Refs. 9 and 17. This method is very suitable for deriving effective Hamiltonians, as we aim at herein. We first perform a unitary transformation on the full Hamilto-

nian, i.e. $H \to e^S H e^{-S} \equiv H_{SW}$, with S an anti-unitary operator so that we get

$$H_{SW} = H_d + H_{SO} + [S, H_d + H_{SO}] \qquad (A1)$$
$$+ \frac{1}{2}[S, [S, H_d + H_{SO}]] + \dots,$$

where $H_d = H_0 + V + H_Z$. We look for the transformation S so that this diagonalizes the full Hamiltonian H in the basis of H_d. In leading order in H_{SO}, we choose S so that $[S, H_0 + V + H_Z] = -(1 - \mathcal{P})H_{SO}$, with the projector operator $\mathcal{P}$ satisfying $\mathcal{P}A = \sum_{E_n = E_m} A_{nm}|m\rangle\langle n|$, $\forall A$, i.e. it projects onto the diagonal part of the Hamiltonian H_d. Keeping the lowest order terms in α and β in the SW transformation, we are left with the effective interaction Hamiltonian H_{SW} that contains the desired spin-spin coupling in the basis of H_d

$$H_{SW} = H_d - \frac{1}{2}\mathcal{P}[S, H_{SO}], \qquad (A2)$$

where $S = (1-\mathcal{P})L_d^{-1}H_{SO}$, with L_d being the Liouvillian superoperator ($L_d A = [H_d, A], \forall A$).

Next we find the explicit expression for the spin-spin coupling due to the second-order term in SOI in Eq. (A2), i.e. $U \equiv \frac{1}{2}[S, H_{SO}]$. We make use of the explicit time-dependent (integral) representation of the Liouvillian $L_d^{-1} = -i\int_0^\infty dt e^{i(L_d + i\eta)t}$ and arrive at

$$U = -\frac{i}{2}\int_0^\infty dt e^{-\eta t}[H_{SO}(t), H_{SO}], \qquad (A3)$$

where $H_{SO}(t) = e^{iL_d t}H_n = e^{iH_d t}H_n e^{-iH_d t}$, and $\eta \to 0^+$ ensures the convergence of the time integration. Heisenberg operators, $\boldsymbol{\sigma}_i(t)$ and $\boldsymbol{p}_i(t)$, are needed in order to calculate U. The former is easy to obtain $\boldsymbol{\sigma}_i(t) = \widehat{\Sigma}_i(t)\boldsymbol{\sigma}_i$, with $\widehat{\Sigma}_i(t)$ given by

$$(\widehat{\Sigma}_i)_{mn}(t) = \delta_{mn}\boldsymbol{l}_i^2 \cos\frac{E_{Zi}t}{2\hbar} + 2(\boldsymbol{l}_i)_m(\boldsymbol{l}_i)_n \sin^2\frac{E_{Zi}t}{4\hbar}$$
$$-\varepsilon_{nmk}(\boldsymbol{l}_i)_k \sin\frac{E_{Zn}t}{2\hbar}, \qquad (A4)$$

with $\boldsymbol{l}_i = \boldsymbol{B}_i/B$. The calculation of $\boldsymbol{p}_i(t)$ consists of solving the system of ordinary differential equations (ODEs)

$$\frac{d}{dt}\boldsymbol{p}_i(t) = -m^*\omega_0^2\boldsymbol{r}_i(t) - \frac{\partial}{\partial\boldsymbol{r}_i}V(\boldsymbol{r}_1(t), \boldsymbol{r}_2(t)), \quad (A5)$$
$$\frac{d}{dt}\boldsymbol{r}_i(t) = \boldsymbol{p}_i(t)/m^*. \qquad (A6)$$

In order to solve this system we expand the electrostatic potential, given in Eq. (3), around the minima to second order in $\boldsymbol{r}_i(t)$. The system of ODEs now reads

$$\frac{d^2}{dt^2}\begin{pmatrix} \boldsymbol{p}_1(t) \\ \boldsymbol{p}_2(t) \end{pmatrix} = -\widehat{\Omega}\begin{pmatrix} \boldsymbol{p}_1(t) \\ \boldsymbol{p}_2(t) \end{pmatrix}, \qquad (A7)$$

$$\widehat{\Omega} = \begin{pmatrix} \omega_x^2 & 0 & & \widehat{\Omega}_{12} \\ 0 & \omega_y^2 & & \\ & & \omega_x^2 & 0 \\ \widehat{\Omega}_{12}^\dagger & & 0 & \omega_y^2 \end{pmatrix}. \qquad (A8)$$
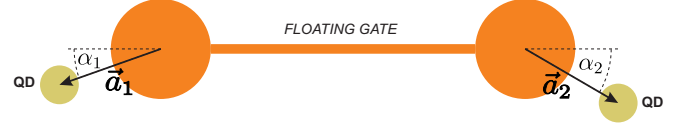

FIG. 8. The misalignment angle α of the two QDs (yellow), defined with respect to the metallic floating gate (orange).

In this approximation only terms $O(\boldsymbol{r}_i^2)$ are retained—this is valid for low lying levels. We ignore the renormalization of the frequencies (ω_x and ω_y) because it gives higher order (in the Coulomb energy) contribution to the effective spin-spin coupling. The coupling between the QDs ($\widehat{\Omega}_{12}$) is given by

$$(\widehat{\Omega}_{12})_{ij} = \pi\alpha_q\alpha_C \left(\frac{\partial q_{ind}}{\partial\tilde{\boldsymbol{r}}_i}\right)\left(\frac{\partial q_{ind}}{\partial\tilde{\boldsymbol{r}}_j}\right)\omega_i\omega_j, \quad (A9)$$

$$(\partial q_{ind}/\partial\boldsymbol{r}_i)_{\boldsymbol{r}=0} = \frac{2R\sqrt{\xi_0^2 - R^2}\boldsymbol{a}_i}{\pi\xi_0^2(2\xi_0^2 - a_0^2 - R^2 - d^2)}, \qquad (A10)$$

where $\alpha_q = C_d/(C_d + C_w)$, $\alpha_C = e^2/(\kappa R\hbar\omega_x)$, and $\tilde{\boldsymbol{r}}_i = \boldsymbol{r}_i/\lambda_i$ (λ_i is the QD size along the i-th direction). $\boldsymbol{a}_i$ are the vectors that define the position of the QDs with respect to the nearby disc center, see Fig. 8. Note that the expressions for the disc (C_d) and wire (C_w) capacitances, *resp.* are given by

$$C_d = 2R/\pi, \qquad (A11)$$
$$C_w = \frac{L}{2\ln(L/R_w)}, \qquad (A12)$$

where R is the radius of the disk, R_w is the radius of the wire and L is the length of the wire.

In order to obtain the solution of Eq. (A8), we note that even a slight ellipticity ($|\omega_x^2 - \omega_y^2| \gg \max[(\widehat{\Omega}_{12})_{xy}^2, (\widehat{\Omega}_{12})_{yx}^2]$) of the QDs causes the motion in the x- and y-direction to be decoupled. Having in mind that $(\widehat{\Omega}_{12})_{yx,xy}^2/\omega_{x,y}^2 \sim 10^{-3} - 10^{-4}$, we conclude that such a ellipticity is unavoidable in realistic experimental devices. Thus, we put off-diagonal elements of the $\widehat{\Omega}_{12}$ matrix to zero and obtain the solutions

$$\boldsymbol{p}_{1,2}^i(t) = \pm\boldsymbol{p}_{xa}^i\cos(\boldsymbol{\omega}_+^i t) + \boldsymbol{p}_{xs}^i\cos(\boldsymbol{\omega}_-^i t) \mp \qquad (A13)$$
$$\mp m^*\boldsymbol{r}_a^i\boldsymbol{\omega}_+^i\sin(\boldsymbol{\omega}_+^i t) - m^*\boldsymbol{r}_s^i\boldsymbol{\omega}_-^i\sin(\boldsymbol{\omega}_-^i t),$$

herein the notation $\boldsymbol{r}_{s,a} = (\boldsymbol{r}_1 \pm \boldsymbol{r}_2)/2$, $\boldsymbol{p}_{s,a} = (\boldsymbol{p}_1 \pm \boldsymbol{p}_2)/2$ and $\boldsymbol{\omega}_\pm = \left(\sqrt{\omega_x^2 \pm (\widehat{\Omega}_{12})_{xx}^2}, \sqrt{\omega_y^2 \pm (\widehat{\Omega}_{12})_{yy}}\right)$ has been introduced. In the previous formula, a subscript of a vector denotes the corresponding component of the vector.

Next, the obtained solutions are inserted into Eq. (A3). Finally, after performing the integration over time one obtains the effective spin-spin coupling for arbitrary orientation of the magnetic field

$$H_{s-s} = \sum_{i=x,y} \frac{m^*\omega_{i,12}^2 E_{Z1}^2(\boldsymbol{l}_1 \times (\boldsymbol{l}_1 \times \boldsymbol{\gamma}_i)) \cdot \boldsymbol{\sigma}_1(\boldsymbol{\sigma}_2 \cdot \boldsymbol{\gamma}_i)}{4(\omega_x^2 - E_{Z1}^2)(\omega_x^2 - E_{Z2}^2)}$$
$$+ 1 \leftrightarrow 2, \qquad (A14)$$

where $\boldsymbol{\gamma}_x = (\beta\cos 2\gamma, -\alpha - \beta\cos 2\gamma, 0)$, $\boldsymbol{\gamma}_y = (\alpha - \beta\sin 2\gamma, -\beta\cos 2\gamma, 0)$, and $\boldsymbol{l}_i = \boldsymbol{B}_i/B$. For simplicity of notation, $\boldsymbol{\gamma}_x$ is referred to as $\boldsymbol{\gamma}$ in the main text.

Few remarks should be main herein for the result embodied in the Eq. (A14). First of all, from Eq. (A10) we see that $\hat{\Omega}_{12} \propto \boldsymbol{a}_1 \otimes \boldsymbol{a}_2$, accordingly, the two terms in the sum of Eq. (A14) are proportional to $\cos\alpha_1 \cos\alpha_2$ and $\sin\alpha_1 \sin\alpha_2$—the angles α_i are being depicted in Fig. 8. When only Rashba SOI is present in the material, the coefficients in front of the two terms are equal and the coupling is proportional to $\boldsymbol{a}_1 \cdot \boldsymbol{a}_2$. This gives yet another efficient switching mechanism thereby, when the QDs are rotated in such a way that the two vectors are orthogonal $(\boldsymbol{a}_1 \cdot \boldsymbol{a}_2 = 0)$[34].

Appendix B: SPIN-SPIN COUPLING - the hybrid system

We start from the Hamiltonian of the system and then apply the Schrieffer-Wolff transformation to remove the first order SOI term (present only in the single QD). The electrostatic potential V is again expanded around the minimum

$$V(\boldsymbol{r}_e, \boldsymbol{r}_1, \boldsymbol{r}_2) = V(\boldsymbol{r}_e, \boldsymbol{r}_1) + V(\boldsymbol{r}_e, \boldsymbol{r}_2) \qquad (B1)$$
$$\approx m^* \sum_{i=e,1,2} (\delta\omega_x^2 x_i^2 + \delta\omega_y^2 y_i^2)$$
$$+ m^*\omega_{x,12}^2 x_e(x_1 + x_2),$$

where $\boldsymbol{r}_e$, $\boldsymbol{r}_1$, and $\boldsymbol{r}_2$ are the coordinates with respect to the local minima for the electron in the single QD, and the two electrons in the DQD, respectively. The terms under the sum only renormalize the frequencies, we do not take them into account, they give only higher order (in the Coulomb energy) contributions to the final results. The last term acts as an electric field on the DQD; as has been shown in the Ref. 15, this leads to a change in the exchange splitting between the singlet and triplet states in the DQD.

$$H = H_0 + H_Z + H_{SO} + \delta\tilde{J}\tilde{x}_e \boldsymbol{S}_1 \cdot \boldsymbol{S}_2, \qquad (B2)$$

where $\delta\tilde{J}$ is given by

$$\delta\tilde{J} = \frac{3}{\sinh(2\tilde{l}^2)} \frac{\omega_{x,12}^2}{\tilde{l}\omega_D^2} \epsilon. \qquad (B3)$$

ω_D is the confinement energy in the DQD, $\tilde{l}$ is the distance between the DQD minima measured in units of a QD size. We assumed that the detuning ϵ is applied to the DQD in order to get the coupling linear in electrostatic coupling.

The Schrieffer-Wolff transformation is given by $S = (L_0 + L_Z + L_H)^{-1} H_{SO}$. Similarly to the previous section, in order to find the inverse Liouvillian we have to solve the system of ODEs

$$\frac{d}{dt} p_{e,x}(t) = -m^*\omega_x^2 x_e(t) - m^*\tilde{J}\boldsymbol{S}_1 \cdot \boldsymbol{S}_2, \qquad (B4)$$

$$\frac{d}{dt} p_{e,y}(t) = -m^*\omega_y^2 y_e(t), \qquad (B5)$$

$$\frac{d}{dt} \boldsymbol{r}_e(t) = \boldsymbol{p}_e(t)/m^*. \qquad (B6)$$

The solution is easily obtained

$$p_e^x(t) = p_e^x \cos(\omega_x t) \qquad (B7)$$
$$- m^*\left(x_e\omega_x + \frac{\tilde{J}}{m^*\omega_x\lambda} \boldsymbol{S}_1 \cdot \boldsymbol{S}_2\right)\sin(\omega_x t),$$

$$p_e^y(t) = p_e^y \cos(\omega_y t) - m^* y_e\omega_y \sin(\omega_y t). \qquad (B8)$$

After integration over time, the S transformation is obtained

$$-iS = \sum_{i=x,y} \frac{m^* r_{e,i}\left(\mu^2 g^2(\boldsymbol{B}\cdot\boldsymbol{\gamma}_i)(\boldsymbol{B}\cdot\boldsymbol{\sigma}) - 4\omega_i^2\boldsymbol{\gamma}_i\cdot\boldsymbol{\sigma}\right)}{8(\omega_i^2 - E_Z^2)}$$
$$+ \frac{\mu g(\boldsymbol{B}\times\boldsymbol{\sigma})\cdot\boldsymbol{\gamma}_i p_{e,i}}{4(\omega_i^2 - E_Z^2)} \qquad (B9)$$
$$+ \frac{\mu^2 g^2(\boldsymbol{B}\cdot\boldsymbol{\gamma}_x)(\boldsymbol{B}\cdot\boldsymbol{\sigma}) - 4\omega_x^2\boldsymbol{\gamma}_x\cdot\boldsymbol{\sigma}}{8\omega_x^2(\omega_x^2 - E_Z^2)\lambda}\delta\tilde{J}\boldsymbol{S}_1 \cdot \boldsymbol{S}_2,$$

The coupling is contained in the $[S, H_Z + \delta\tilde{J}\tilde{x}_e\boldsymbol{S}_1 \cdot \boldsymbol{S}_2]$ term

$$H_{S-s} = \frac{3\mu g\,\delta\tilde{J}(\boldsymbol{\gamma}_x \times \boldsymbol{B})\cdot\boldsymbol{\sigma}}{4(\omega_x^2 - E_Z^2)\lambda}(\boldsymbol{S}_1 \cdot \boldsymbol{S}_2). \qquad (B10)$$

By rewriting the last equation in the pseudo-spin space the generalization for Eq. (12) for arbitrary magnetic field orientation is obtained.

Appendix C: Implementation of two-qubit gates

Two qubits interacting via the floating gate evolve according to the Hamiltonian $H = H_{S-S} + E_Z(\sigma_z^1 + \sigma_z^2)$, the sum of the qubit-qubit coupling and Zeeman term. In general these contributions do not commute, making it difficult to use the evolution to implement standard entangling gates. However, when the field is perpendicular to the 2DEG substrate, H_{S-S} takes the form of Eq. (8) which can be decomposed into two terms as follows,

$$H_{S-S} = J_{12}(\Gamma_1 - i\Gamma_2\sigma_z^1)(\sigma_x^1\sigma_x^2 - \sigma_y^1\sigma_y^2)/2$$
$$+ J_{12}|\gamma_{\mathbf{x}}|^2(\sigma_x^1\sigma_x^2 + \sigma_y^1\sigma_y^2)/2. \qquad (C1)$$

Here $\Gamma_1 = ((\gamma_x)_x^2 - (\gamma_x)_y^2)$ and $\Gamma_2 = (\gamma_x)_x(\gamma_x)_y$. The first of these two terms anticommutes with the Zeeman term, whereas the second commutes. As such, when $E_Z \gg J_{12}|\gamma_{\mathbf{x}}|^2$, H_{S-S} can be approximated by the second term alone,

$$H_{S-S} \approx H'_{S-S} = \frac{J_{12}|\gamma_x|^2}{2}(\sigma_x^1\sigma_x^2 + \sigma_y^1\sigma_y^2), \qquad (C2)$$

$$H \approx H' = H'_{S-S} + E_z(\sigma_z^1 + \sigma_z^2)/2. \qquad (C3)$$

With this approximation, the coupling and Zeeman terms in H' now commute.

We consider the implementation of the gate $\sqrt{\sigma_x\sigma_x} = \exp(-i\sigma_x^1\sigma_x^2\pi/4)$, which is locally equivalent to a CNOT. The Hamiltonian H' already contains a $\sigma_x^1\sigma_x^2$ term, so implementation of the $\sqrt{\sigma_x\sigma_x}$ gate requires only that the effects of the other terms be removed by appropriate local rotations. Two possible sequences that can be used to achieve this are,

$$\sqrt{\sigma_x\sigma_x} = e^{i(\sigma_z^1+\sigma_z^2)E_z t}e^{-iH't}$$
$$\sigma_x^1 e^{i(\sigma_z^1+\sigma_z^2)E_z t}e^{-iH't}\sigma_x^1, \quad \text{(C4)}$$

$$\sqrt{\sigma_x\sigma_x} = \sigma_x^2\, e^{-iH't/2}\, \sigma_x^1\sigma_x^2\, e^{-iH't/2}$$
$$\sigma_x^2\, e^{-iH't/2}\, \sigma_x^1\sigma_x^2\, e^{-iH't/2}, \quad \text{(C5)}$$

where $t = \pi/(4J_{12}|\boldsymbol{\gamma}|^2)$. The first sequence requires two applications of the qubit-qubit coupling, whereas the second requires four. The main difference is that the former removes the effects of the field through the application of corresponding z-rotations after each application of H', whereas the latter uses x-rotations to negate the sign of the field terms and additional applications of H' to cancel them out. The former is therefore simpler to implement, however the latter method will also cancel terms not taken into account in the approximation.

Once the $\sqrt{\sigma_x\sigma_x}$ has been implemented using either of the above sequences, the CNOT gate, C, may be applied using the appropriate local rotations,

$$C = \sqrt{\sigma_z^1}\,\sqrt{\sigma_x^2}\,\mathcal{H}^1\,\sqrt{\sigma_x\sigma_x}\,\mathcal{H}^1. \quad \text{(C6)}$$

Here $\mathcal{H}$ denotes the single qubit Hadamard rotation.

Since H' is an approximation of H, the above sequences will yield approximate CNOTs, C', when used with the full Hamiltonian. The success of the sequences therefore depends on the fidelity of the gates, $F(C')$. Ideally this would be defined using a minimization over all possible states of two qubits. However, to characterize the fidelity of an imperfect CNOT it is sufficient to consider the following four logical states of two qubits: $|+,0\rangle, |+,1\rangle, |-,0\rangle$, and $|-,1\rangle$. These are product states which, when acted upon by a perfect CNOT, become the four maximally entangled Bell states $|\Phi^+\rangle, |\Psi^+\rangle, |\Phi^-\rangle$, and $|\Psi^-\rangle$, respectively. As such, the fidelity of an imperfect CNOT may be defined,

$$F(C') = \min_{i\in\{+,-\},j\in\{0,1\}} |\langle i,j|C^\dagger C'|i,j\rangle|^2. \quad \text{(C7)}$$

The choice of basis used here ensures that $F(C')$ gives a good characterization of the properties of C' in comparison to a perfect CNOT, especially for the required task of generating entanglement.

In a realistic parameter regime it can be expected that $(\boldsymbol{\gamma}_x)_x$ and $(\boldsymbol{\gamma}_x)_y$ will be of the same order, and the qubit-qubit coupling will be a few orders of magnitude less than the Zeeman terms. To get a rough idea of what fidelities can be achieved in such cases using the schemes proposed, we average over 10^4 samples for which $(\boldsymbol{\gamma}_x)_y$ is randomly assigned values between $(\boldsymbol{\gamma}_x)_x/2$ and $3(\boldsymbol{\gamma}_x)_x/2$ according to the uniform distribution, and $J_{12}(\boldsymbol{\gamma}_x)_x/E_Z = 0.1$. This yields values of 99.33% and 99.91% for the sequences of Eq. (C4) and Eq. (C5), respectively. For $J_{12}(\boldsymbol{\gamma}_x)_x/E_Z = 0.01$ these improve, becoming 99.993% and 99.998%, respectively.

To compare these values to the thresholds found in schemes for quantum computation, we must first note that imperfect CNOTs in these cases are usually modelled by the perfect implementation of the gate followed by depolarizing noise at a certain probability. It is known that such noisy CNOTs can be used for quantum computation in the surface code if the depolarizing probability is less than 1.1%.[6] This corresponds to a fidelity, according to the definition above, of 99.17%. The fidelities that may be achieved in the schemes proposed here are well above this value and hence, though they do not correspond to the same noise model, we can expect these gates to be equally suitable for fault-tolerant quantum computation.

[1] R. Hanson, L. P. Kouwenhoven, J. R. Petta, S. Tarucha, and L. M. K. Vandersypen, Rev. Mod. Phys. **79**, 1217 (2007).

[2] H. Bluhm, S. Foletti, I. Neder, M. Rudner, D. Mahalu, V. Umansky, and A. Yacoby, Nat Phys **7**, 109 (2011).

[3] A. M. Childs, H. L. Haselgrove, and M. A. Nielsen, Phys. Rev. A **68**, 052311 (2003).

[4] D. Loss and D. P. DiVincenzo, Phys. Rev. A **57**, 120 (1998).

[5] R. Raussendorf and J. Harrington, Phys. Rev. Lett. **98**, 190504 (2007).

[6] D. S. Wang, A. G. Fowler, and L. C. L. Hollenberg, Phys. Rev. A **83**, 020302 (2011).

[7] J. Levy, Phys. Rev. Lett. **89**, 147902 (2002).

[8] C. Flindt, A. S. Sørensen, and K. Flensberg, Phys. Rev. Lett. **97**, 240501 (2006).

[9] M. Trif, V. N. Golovach, and D. Loss, Phys. Rev. B **75**, 085307 (2007).

[10] D. Stepanenko and G. Burkard, Phys. Rev. B **75**, 085324 (2007).

[11] A. C. Johnson, J. R. Petta, J. M. Taylor, A. Yacoby, M. D. Lukin, C. M. Marcus, M. P. Hanson, and A. C. Gossard, Nature **435**, 925 (2005).

[12] I. H. Chan, R. M. Westervelt, K. D. Maranowski, and A. C. Gossard, Appl. Phys. Lett. **80**, 1818 (2002).

[13] F. Kuemmeth, S. Ilani, D. C. Ralph, and P. L. McEuen, Nature **452**, 448 (2008).

[14] J. Sten, J. Electrostatics **64**, 647 (2006).

[15] G. Burkard, D. Loss, and D. P. DiVincenzo, Phys. Rev. B **59**, 2070 (1999).

[16] J. H. Van Vleck, Phys. Rev. **57**, 426 (1940).

[17] V. N. Golovach, A. Khaetskii, and D. Loss, Phys. Rev. Lett. **93**, 016601 (2004).

[18] R. Zak, B. Rothlisberger, S. Chesi, and D. Loss, Riv. Nuovo Cimento **33**, 345 (2010).

[19] D. P. DiVincenzo, Phys. Scr. **T137**, 014020 (2009).

[20] F. H. L. Koppens, C. Buizert, K. J. Tielrooij, I. T. Vink, K. C. Nowack, T. Meunier, L. P. Kouwenhoven, and L. M. K. Vandersypen, Nature **442**, 766 (2006).

[21] V. N. Golovach, M. Borhani, and D. Loss, Phys. Rev. B **74**, 165319 (2006).

[22] K. C. Nowack, F. H. L. Koppens, Y. V. Nazarov, and L. M. K. Vandersypen, Science **318**, 1430 (2007).

[23] S. Nadj-Perge, S. M. Frolov, E. P. A. M. Bakkers, and L. P. Kouwenhoven, Nature **468**, 1084 (2011).

[24] C. Fasth, F. A., L. Samuleson, V. N. Golovach, and D. Loss, Phys. Rev. Lett. **98**, 266801 (2007).

[25] Y. Hu, H. O. H. Churchill, D. J. Reilly, J. Xiang, C. M. Lieber, and C. M. Marcus, Nat. Nanotech. **2**, 622 (2007).

[26] C. Klöffel, M. Trif, and D. Loss, arXiv:1107.4870 (2011).

[27] F. Kuemmeth, S. Ilani, D. C. Ralph, and P. L. McEuen, Nature **452**, 448 (2008).

[28] D. V. Bulaev, B. Trauzettel, and D. Loss, Phys. Rev. B **77**, 235301 (2008).

[29] H. O. H. Churchill, A. J. Bestwick, J. W. Harlow, J. Kuemmeth, D. Marcos, C. H. Stwertka, S. K. Watson, and C. M. Marcus, Nat. Phys. **5**, 321 (2009).

[30] J. Klinovaja, M. J. Schmidt, B. Braunecker, and D. Loss, Phys. Rev. Lett. **106**, 156809 (2011).

[31] J. Fischer and D. Loss, Science **324**, 1277 (2009).

[32] S. Amasha, K. MacLean, I. P. Radu, D. M. Zumbühl, M. A. Kastner, M. P. Hanson, and A. C. Gossard, Phys. Rev. Lett. **100**, 046803 (2008).

[33] F. Marquardt and V. A. Abalmassov, Phys. Rev. B **71**, 165325 (2005).

[34] Coupling is zero up to the small terms $O\left((\hat{\Omega}_{12})^2_{xy,yx}/|\omega_x^2 - \omega_y^2|\right)$.